



Pergamon

Available online at www.sciencedirect.com

SCIENCE @ DIRECT®

Acta Materialia 51 (2003) 6277–6290



www.actamat-journals.com

Yielding behavior of aluminum-rich single crystalline γ -TiAl

Marc Zupan^{a,*}, K.J. Hemker^b

^a Department of Engineering, University of Cambridge, Trumpington Street, Cambridge CB2 1PZ, UK

^b Department of Mechanical Engineering, The Johns Hopkins University, Baltimore, MD 21218, USA

Received 7 April 2003; received in revised form 29 July 2003; accepted 29 July 2003

Abstract

The yielding behavior of Al-rich single crystalline γ -Ti 55.5 at% Al has been measured along near [0 0 1], [0 1 0] and $[\bar{1} 1 0]$ orientations in both tension and compression and as function of temperature. All three orientations displayed anomalous yielding and a pronounced tension/compression asymmetry. The relative strength of the material, location of the anomalous yielding peak, and tension/compression asymmetry are all orientation dependent. A micromechanical superdislocation model addressing crystal geometry, sense of the applied load, Escaig forces and the Yoo torque is presented to explain the observed experimental results.

© 2003 Acta Materialia Inc. Published by Elsevier Ltd. All rights reserved.

Keywords: Microsample; Titanium aluminides; High temperature deformation; Single crystal; Dislocations

1. Introduction

Physical and mechanical properties, such as low density, high thermal conductivity and high temperature strength, make γ -based titanium aluminide alloys attractive candidates for high temperature weight critical applications [1,2]. Two-phase, α_2 -Ti₃Al+ γ -TiAl, microstructures are being developed to provide an overall balance of properties. It is well understood that the γ -phase carries the vast majority of deformation in two-phase alloys, but a detailed understanding of the mechanical behavior of single-phase γ -TiAl has not been forthcoming. One of the limitations in developing

such an understanding has been the difficulty in obtaining single crystalline γ -TiAl. However, the development of optical float-zone crystal growing techniques has led to the availability of small crystals and related compressive yielding studies of Al-rich γ -TiAl.

γ -TiAl possesses the L1₀ face-centered tetragonal crystal structure that is slightly tetragonal, $c/a \sim 1.02$ [3,4] and highly anisotropic with different atomic species along the [0 0 1] axis. The reduced symmetry of the L1₀ structure results in ordinary dislocations, $\mathbf{b}_{\text{ord}} = 1/2 \langle 1 1 0 \rangle$, and superdislocations, $\mathbf{b}_{\text{super}} = \langle 1 0 1 \rangle$. The superdislocation reduces its energy by first dissociating into two superpartial dislocations, $\mathbf{b}_{\text{sp}} = 1/2 \langle 1 0 1 \rangle$, and further to four Shockley partial dislocations of $\mathbf{b}_{\text{Shockley}} = 1/6 \langle 1 1 2 \rangle$ or $\mathbf{b}_{\text{Shockley}} = 1/6 \langle 2 1 1 \rangle$. The entire superdislocation decomposition can be written as:

* Corresponding author. Tel.: +44-1223-339883; fax: +44-1223-332662.

E-mail address: mpz20@eng.cam.ac.uk (M. Zupan).

$$\begin{aligned}
 < 0 1 1 \rangle \rightarrow 1/6 < 1 2 1 \rangle + \text{CSF} + 1/6 \\
 < 1 1 2 \rangle + \text{APB} + 1/6[1 2 1] + \text{SISF} \quad (1) \\
 + 1/6 < 1 1 2 \rangle
 \end{aligned}$$

Three different faults, super intrinsic stacking fault (SISF), antiphase boundary (APB), and complex stacking fault (CSF) are the products of this dissociation.

Fu and Yoo [5], Woodward et al. [6], Simmons et al. [7], Rao et al. [8], Panova and Farkas [9], Girshik and Vitek [10], and Schoeck et al. [11] have all calculated the planar stacking fault energies in γ -TiAl. Hug et al. [12] and Wiezorek and Humphreys [13] have made experimental weak-beam TEM measurements of the stacking faults. The experimental and theoretical studies all conclude that the APB and CSF energies are substantially higher than the SISF energy.

Subsequent calculations of the partial dislocation separations on the $\{1 1 1\}$ plane [5,8,11,14], predict a non-symmetric planar dissociation. The relative partial dislocation separations are shown schematically in Fig. 1 with the Shockley partial dislocations separated by the SISF widely spread on the glide plane and the two Shockley partials bounding the CSF comprising a very compact structure. This strong asymmetry has led some investigators to describe the dislocation dissociation as effectively being threefold written: $< 0 1 1 \rangle \rightarrow 1/6 < 1 1 2 \rangle + \text{SISF} + 1/6 < 1 2 1 \rangle + \text{APB} + 1/2 < 0 1 1 \rangle$ [15]. The chemical and physical asymmetry of the Shockley partial dislocations suggest that the macroscopic mechanical properties resulting from superdislocation motion may differ based on the direction of motion of the dislocation through the crystal and whether the SISF or CSF is leading.

The availability of relatively small Al-rich γ -



Fig. 1. Planar dissociation of a superdislocation ($\mathbf{b} = < 1 0 1 \rangle$) into four Shockley partial dislocations, a superlattice intrinsic stacking fault (SISF), an antiphase boundary (APB), and a complex stacking fault (CSF).

TiAl single crystals has permitted measurements of the alloy's compressive flow strength as a function of temperature for a number of crystallographic orientations. The first compression studies by Kawabata et al. [16–19], measured the flow strength between 4.2 and 1273 K and documented a positive flow stress anomaly at the three corners of the extended standard stereographic projection triangle, namely $[0 0 1]$, $[0 1 0]$ and $[\bar{1} 1 0]$. A comprehensive study by Inui et al. [20] tested single crystals of Ti 56 at% Al along seven different loading axes and concluded that anomalous yielding is attributed to screw oriented superdislocations adopting a locked configuration for all orientations except those within a few degrees of the $[0 2 1]$ orientation.

Binary Ti 56 at% Al single crystals tested along $[0 1 0]$ by Stucke et al. [21] demonstrated that deformation is not thermally reversible because dislocations become “permanently locked”. Moreover, the same group tested $[0 0 1]$ crystals and linked anomalous flow behavior with superdislocations cross-slip locking [22]. Wang et al. [23] compressed Ti 56 at% Al crystals oriented for single slip and also observed cross-slipped superdislocations dominating the deformed structure. For the same alloy and orientation Wang et al. [24] examined the superdislocation core structure and observed superpartial dislocations dissociated on two different octahedral planes forming an acute angle “roof-type” configuration. Compression experiments on Ti 54.4 at% Al by Jiao et al. [25] also linked the flow stress anomaly to the operation of superdislocations up to the peak temperature. The work by Gregori and Veyssiere [15] for Ti 54.4 at% Al concurred with the earlier works and established that trailing partial dislocation cross-slip is responsible for superdislocations locking event causing anomalous yielding.

In near stoichiometric polycrystalline alloys Viguier et al. [26] and Sriram et al. [27] reported ordinary dislocation, not superdislocation, activity during anomalous yielding. In these alloys anomalous yielding is related to the localized pinning and unzipping of ordinary dislocations. A study by Bird et al. [28] on Ti 54 at% Al at the $[\bar{3} 16 15]$ orientation concluded anomalous yielding results from the increasing cross-slip frequency of ordinary

screw dislocation segments. Inui et al. [20], Feng and Whang [29], and Gregori and Veysiere [15], all reported ordinary dislocation activity in Al-rich single crystal γ -TiAl is limited to a very small region of orientations near the [0 2 1] crystallographic axis. At all other orientations, superdislocation activity dominates the yielding behavior of Al-rich single crystalline γ -TiAl.

The compression studies of Al-rich single crystalline γ -TiAl may be summarized as follows. The orientations and alloys studied exhibit a marked compressive flow strength anomaly. The magnitude and temperature of the anomalous peak is orientation dependent and cannot be explained with Schmid's law. TEM studies established the activity of superdislocations in this anomalous regime, but the critical resolved shear stress (CRSS) acting on superdislocations does not collapse to a single value.

The yield strength anomaly, orientation dependence, and tension/compression asymmetry exhibited by Ni₃Al has been successfully modeled by Paidar et al. [30] using the single crystalline tension and compression experiments of Umakoshi et al. [31] as the basis for their model. The scope of the current study parallels what has been done for Ni₃Al. The tensile and compressive flow strength of single crystalline γ -TiAl have been measured as a function of temperature for three orientations. The observed flow strength behavior is compared with literature data at similar orientations and temperatures, and the source of the observed yielding anomaly, orientation dependence and tension/compression asymmetry is explored with a micromechanical dislocation model.

2. Experimental methods

Single crystals with diameters of less than 10 mm were grown using an optical float zone furnace. A binary composition of Ti 55.5 at% Al, nominally γ -TiAl, was used to assure that the alloy passed directly from the liquid phase to the γ -phase field upon cooling. The as-grown single crystal rods were subsequently quartz encapsulated and homogenized at 1573 K for 24 h, furnace cooled to 1273 K, held for 100 h and finally furnace

cooled to room temperature. This heat treatment was performed to remove excess point defects and compositional inhomogeneities [22]. Single crystal quality was checked using back reflection Laue X-ray diffraction, and electron diffraction was implemented to discern the chemical anisotropy, which lies along the [0 0 1] direction in the L1₀ structure. All specimens were machined by sinking electro-discharge machining (EDM). The faces of the microsamples were mechanically polished using diamond paper, and reflective Pt markers were placed in the gage of the microsamples using a focused ion beam.

The microsample tensile testing machine and interferometric strain displacement gage (ISDG) used in this investigation follow the designs of Sharpe [32,33] and high temperature modifications of Zupan et al. [34,35]. Self-aligning grips match the ends of bowtie shaped specimens and hold the specimens in place. A linear air bearing insures proper alignment of the load frame, greatly reduces friction in the loading mechanism, and permits accurate measurement of the load with an in-line miniature load cell. Loading is accomplished through the use of a piezoelectric actuator that allowed for precise stroke-controlled experiments. The microsamples were heated to and maintained at the test temperatures with self-resistance heating (DC voltages of 5 V and currents of 5–8 A), and the temperature was monitored throughout the experiments with a two-color optical pyrometer.

Single crystalline microsamples of γ -TiAl were tested with loading axes near the [0 0 1], [0 1 0] and $[\bar{1} 1 0]$ crystallographic orientations. The loading axes were purposely chosen to be near those of Kawabata et al. [16–19], Stucke et al. [21,22], Inui et al. [20], and Gregori and Veysiere [15]. The $[\bar{1} 1 0]$ and [0 0 1] orientations were chosen to explore a predicted tension/compression asymmetry between the two orientations caused by twinning [20]. The tension or compression axes were located $\sim 4^\circ$ off the exact crystal orientations to prevent multiple slip from occurring at the high symmetry orientations. A single-slip direction between the three possible deformation mechanisms (i.e. ordinary dislocations, superdislocations, and twinning) had a significantly higher Schmid factor compared to the other slip systems.

Microsamples were deformed in both tension and compression, at a strain rate of 10^{-4} s^{-1} , and over the temperature range of 723–1273 K. The specimens were loaded monotonically until a minimum of 0.2% plastic strain was induced then unloaded. The alloy yield strength was identified using the 0.2% offset method, and specimens were inspected after testing to ensure that plastic deformation had occurred. In the following figures when no unloading curve is displayed, the data represents the total plastic strain achieved before failure. The Young's modulus (e) and coefficient of thermal expansion (CTE) was measured as a function of temperature and crystal orientation during the initial heating-up portion of the experiments. Both physical quantities were found to have the same absolute values and temperature dependence as values calculated from the stiffness matrix $[C_{ij}]$ measured by He et al. [36], providing validity to the stress and strain measurements and microsample experimental technique reported in [37].

3. Experimental results

3.1. Compressive flow strength

Compression test results for the near $[001]$, $[010]$ and $[\bar{1}10]$ orientations are plotted in Fig. 2. The measured 0.2% compressive flow stress has been multiplied by the largest Schmid factor for superdislocation slip because TEM observations of crystals deformed at similar orientations and temperatures reported the prevalence of superdislocation activity [15,19–25]. The compression microsample flow strength measurements and resulting CRSS are presented in Table 1. The CRSS measurements of this study are plotted as a function of temperature with previously published data [15–22] in Fig. 3. The fact the current results overlay previously published compression data attests to the validity of the microsample testing technique. The plots reveal a marked flow strength anomaly for all three orientations tested, with the temperature and magnitude of the stress peak dependent on crystal orientation. The CRSS data does not collapse to one value as would be predicted by Schmid's law. The crystals deformed by

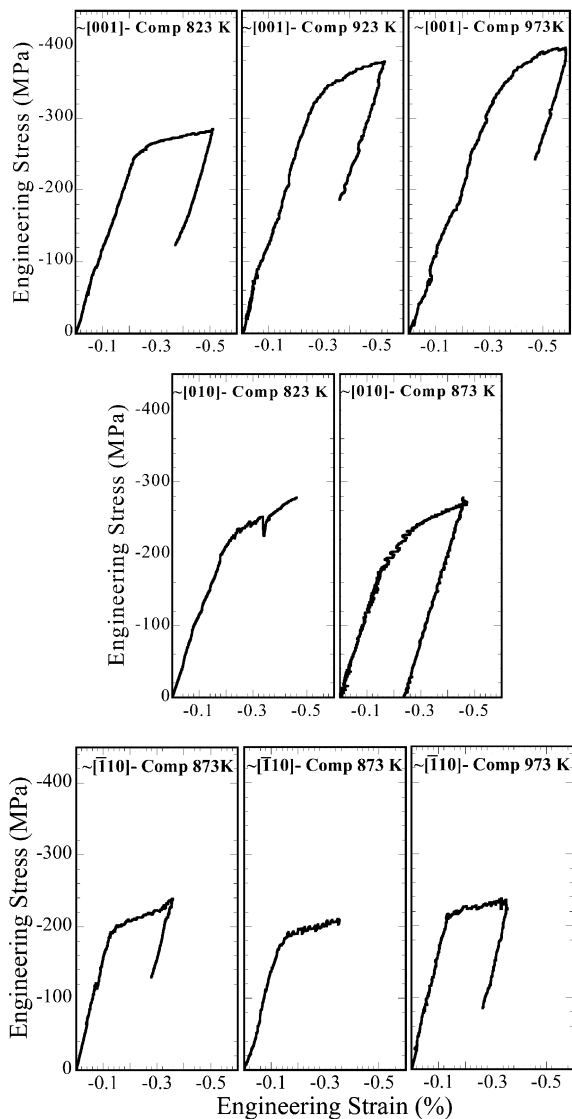


Fig. 2. Compression results for the near $[001]$, $[010]$ and $[\bar{1}10]$ orientations of single crystalline γ -TiAl as a function of temperature. The 0.2% flow strength for this alloys have been extracted from these curves and are displayed in Table 1. The Young's moduli of the loading and unloading curves have been measured and are in good agreement with each other.

Inui et al. [20] did not receive a homogenization heat treatment and the scatter in that data may be attributed to point defects in the as-grown crystals, but it is encouraging to note the trends and absolute values of that study mimics the others.

Table 1

Microsample compression flow stress measurements for single crystalline γ -TiAl for the [0 0 1], [0 1 0] and $[-1 1 0]$ crystallographic orientations as a function of temperature. Measurements in italics were made during reversed cycle loading experiments

Axis	Slip system	Temperature (K)	σ (0.2%) (MPa)	CRSS b_{super} (MPa)
[0 0 1]	(1 1 1) < -1 0 1]	823	278	119
		923	376	160
		973	388, 391, 361	167
[0 1 0]	(-1 1 -1) < 0 1 1]	823	270	114
		873	264	113
[-1 1 0]	(-1 1 1) < 0 -1 1]	873	212, 208, 219, 206	91
		973	231, 234	99

3.2. Tensile flow strength

Tensile tests along the near [0 0 1] orientation covered a temperature range of 723–1273 K. Fig. 4 displays the stress–strain curves as a function of temperature and the measured 0.2% flow strength and CRSS values are reported in Table 2. Anomalous yielding behavior was observed up to a peak temperature of 1123 K followed by a rapid decrease in flow strength beyond the peak. To the authors' knowledge no other tensile flow strength measurements exist for single crystals of γ -TiAl. The [0 0 1] tensile flow strength is presented as a function of temperature and compared with the compression results of this work and the literature [15–20,22] in Fig. 5. A pronounced tension/compression asymmetry exists for the near [0 0 1] orientation. The compressive strength is significantly higher than the tensile strength, and the anomalous yielding peak occurs at a lower temperature in compression. These observations suggest that for the [0 0 1] orientation the obstacle responsible for anomalous yielding has a lower activation energy in compression than tension.

Fig. 6 gives the tensile results for the near [0 1 0] tensile axis, and the measured yield strengths and CRSS are reported in Table 2. The flow strength was found to rise with temperature to a peak at ~400 MPa for tests at 973 and 1073 K. After the peak the tensile flow strength drops off precipitously to below 100 MPa at 1173 K. The [0 1 0] tensile flow strength values are plotted in Fig. 7 with previously published compression results [15–21]. As for the near [0 0 1] results, the [0 1 0] data exhibits a marked tension/compression asym-

metry. Unlike the [0 0 1], the flow strength in tension is higher relative to the compressive flow strength for the [0 1 0] orientation. The temperature dependence of the [0 1 0] peaks is also reversed as compared to [0 0 1] observations. The results indicate that the magnitude of the yielding anomaly, the temperature at which that it occurs, and the tension/compression flow strength ratio are all orientation dependent.

The $[\bar{1} 1 0]$ crystal orientation was tested in tension at 873, 973 and 1100 K, Fig. 8. The measured flow stress and CRSS are listed in Table 2. The stress–strain curves suggest that the peak tensile strength is located near 973 K. Fig. 9 is a composite plot of tensile and compressive data of this study and literature values [16–20]. Similar to the [0 1 0] axis, the flow strength measurements are higher in tension than compression, and the tensile peak is located at lower temperatures. Similar to [0 0 1], the onset of anomalous yielding is observed at a lower temperature for the sense of applied load that results in larger relative yield strengths.

3.3. Reversed-cycle loading experiments

Reversed-cycle loading experiments designed to definitively measure the tension/compression asymmetry of yielding on an individual sample were conducted along the [0 0 1] and $[\bar{1} 1 0]$ orientations. The orientations were selected to explore the possible asymmetry derived from twinning [20], and to confirm the measurable tension–compression asymmetry results of the monotonically loaded specimens. Cyclic loading experiments

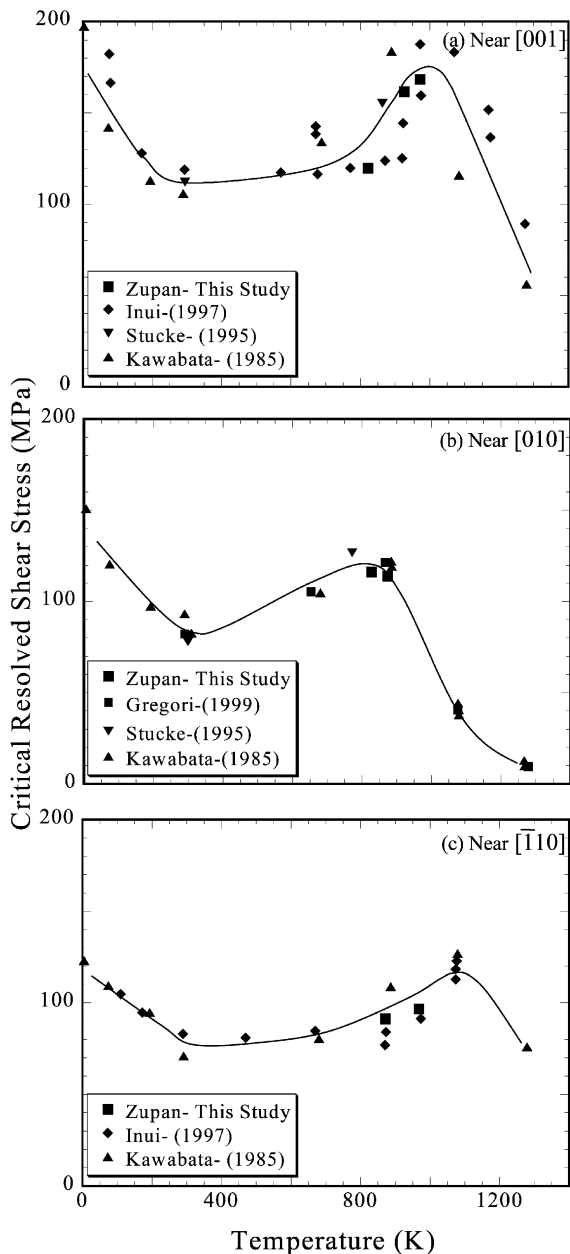


Fig. 3. CRSS for superdislocations as a function of temperature for near [0 0 1], [0 1 0] and $[\bar{1} 1 0]$ single crystals in compression. The microsample data trends and absolute values are in agreement with literature values plotted. For each orientation anomalous yielding is observed, however, the location of the anomalous peak and its magnitude are both dependent on orientation.

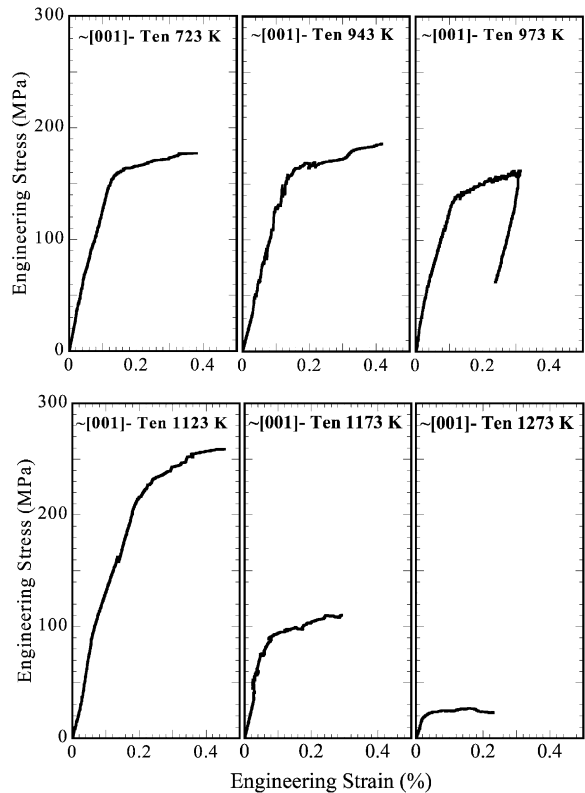


Fig. 4. Single crystalline γ -TiAl tension stress–strain results for near [0 0 1] oriented crystals. Each of the specimens achieved a minimum of 0.2% strain. The 0.2% flow strength was measured from each curve and is reported in Table 2.

were conducted in two stages: first a microsample was loaded in compression to approximately 0.2% plastic strain, unloaded and reloaded in tension until it yielded a second time. The second part of the experiment is to deform a virgin specimen at the same temperature to yielding in tension followed by compressive yielding. The tests were conducted in the anomalous yielding regime to link the deformation mechanism to the anomaly.

Fig. 10 shows the stress–strain curves for [0 0 1] microsamples that were obtained in single cycle loading experiments at 973 K. The first microsample yielded at a compressive stress of 391 MPa on first loading and a tensile stress of 214 MPa when reloaded in tension, Fig. 10(a). The second microsample was loaded in tension and yielded at 186 MPa, after which the load was reversed and the microsample yielded a second time in com-

Table 2

Microsample tension flow stress measurements for single crystalline γ -TiAl along the [0 0 1], [0 1 0] and $[\bar{1}10]$ crystallographic orientations. Measurements in italics were made during reversed cycle loading experiments

Axis	Slip system	Temperature (K)	σ (0.2%) (MPa)	CRSS b_{super} (MPa)
[0 0 1]	(1 1 1) < -1 0 1]	723	177	76
		943	181	77
		973	168, <i>186, 214</i>	81
		1123	256	110
		1173	109	46
		1273	30	12
[0 1 0]	(-1 1 -1) < 0 1 1]	823	291	123
		973	400	170
		1073	401	170
		1173	70, 76	31
[-1 1 0]	(-1 1 1) < 0 -1 1]	873	277, 291, <i>284, 300</i>	124
		973	397, 371, 388	165
		1100	87	37

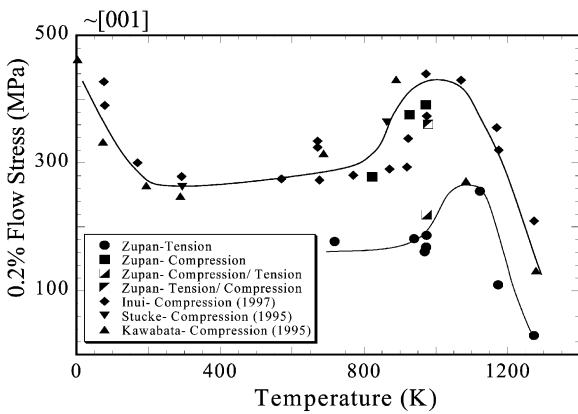


Fig. 5. Tension and compression 0.2% yield strength as a function of temperature for [0 0 1] crystallographic orientation. A flow strength anomaly is observed for both tension and compression in this alloy, and the plot shows a measurable tension/compression asymmetry. The yield strength in compression is larger than in tension and the onset of anomalous yield occurs at a lower temperature in compression.

pression at 361 MPa. Outside of the usual work hardening from the previous cycle and experimental error, the tensile and compressive flow strength measurements are the same between the two experiments. The difference in the two yield values is indicative of the tension/compression asymmetry that is inherent to this alloy. Additional cyclic loading experiments were conducted with near $[\bar{1}10]$ microsamples at 873 and 973 K.

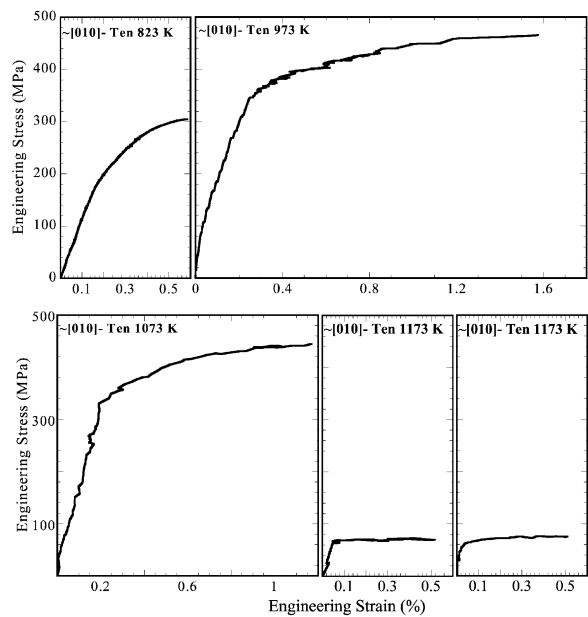


Fig. 6. [0 1 0] tensile stress–strain curves for single crystal γ -TiAl. Of the three orientations tested in this study, the [0 1 0] crystallographic orientation displayed the largest average strain to failure in tension.

Results from the 873 K experiments are displayed in Fig. 11. The $[\bar{1}10]$ reversed cycle experiments also exhibited a pronounced tension/compression asymmetry; with comparable flow strength levels measured between the cyclic tests.

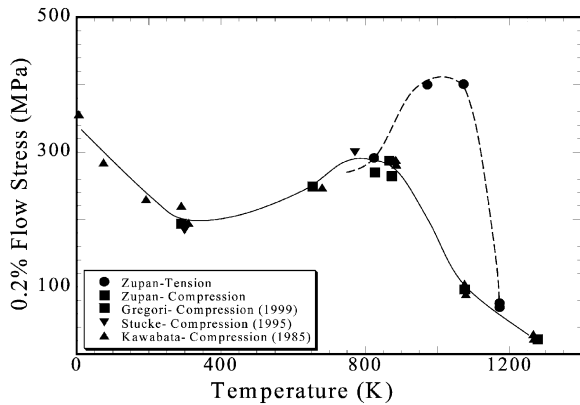


Fig. 7. 0.2% flow stress as a function of temperature for the near $[0\ 1\ 0]$ orientation in tension and compression. The tensile sense of applied load resulted in a higher flow strength relative to compression. This finding is reversed from what was measured for $[0\ 0\ 1]$. Furthermore, the onset of anomalous yielding occurred at a lower temperature for compression.

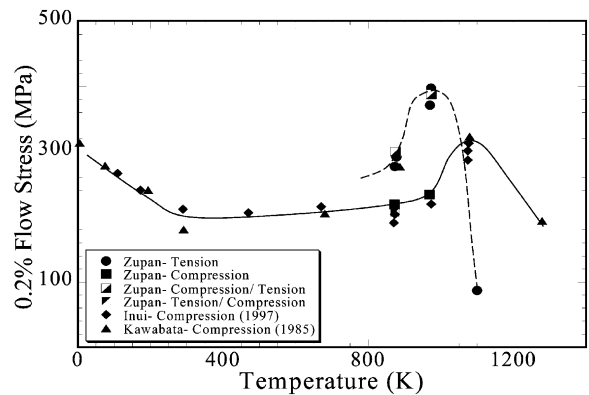


Fig. 9. Flow strength vs. temperature for the $[\bar{1}\ 1\ 0]$ oriented single crystals of γ -TiAl tested in tension and compression. The orientation displays a flow strength anomaly in both tension and compression. A tension/compression asymmetry similar to the one observed for the $[0\ 1\ 0]$ oriented crystals has been measured with tension being the hard mode of deformation.

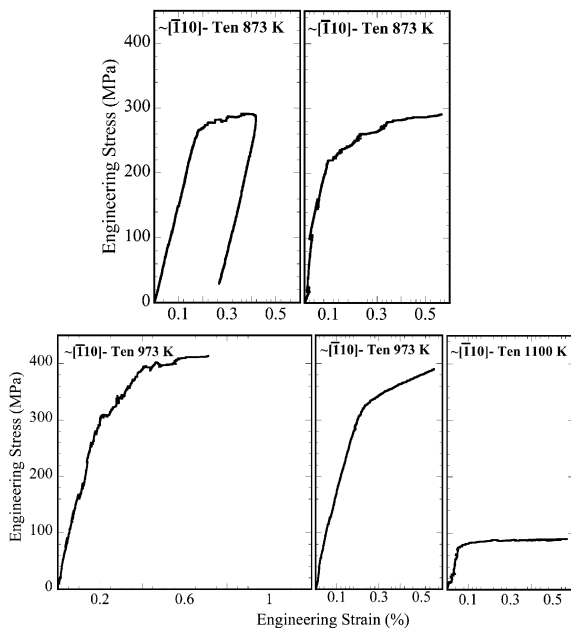


Fig. 8. $[\bar{1}\ 1\ 0]$ tensile result for single crystal γ -TiAl. The one specimen was purposely unloaded and the Young's moduli measured from the loading and unloading curves were in good agreement. The measurement illustrates that micro-cracking had not occurred in the specimen. The other curves represent the strain to failure for this orientation and temperature.

The 0.2% flow strength values of each reversed loading experiment are included in Figs. 5 and 9 and Table 1 (compression) and Table 2 (tension) with the monotonically loaded data. It is noted that the flow strength measurements from the fully reversed cyclic-loading specimens fall within the virgin sample data scatter and display the same tension/compression asymmetry as the monotonic tests. This result suggests that the same deformation mode was active in both tension and compression, and the unidirectional deformation mechanism, twinning, is not active since anomalous yielding was observed in both tension and compression.

4. Yielding model

The yielding behavior of Al-rich single crystalline γ -TiAl is presented in the previous section as a function of orientation, temperature and applied load. The experimental results of this study are summarized and compared with literature values in Figs. 5, 7, and 9. The salient attributes of the deformation in the anomalous regime are summarized below and will be used to construct a micromechanical dislocation model for the measured yield response.

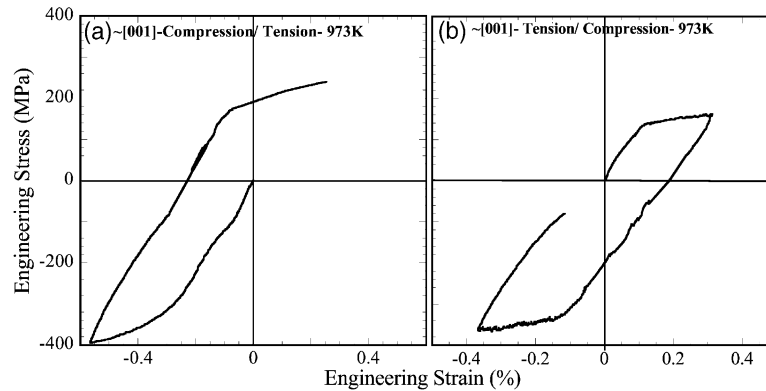


Fig. 10. Stress–strain curves for the cyclic loading of a single crystal along the near $[0\ 0\ 1]$ orientation. (a) In the first cyclic loading excursion the microsample yielded at 391 MPa in compression and 214 MPa in tension. (b) At the same temperature, a new microsample was first loaded in tension and found to yield at 186 MPa and then compressed and observed to yield at 361 MPa.

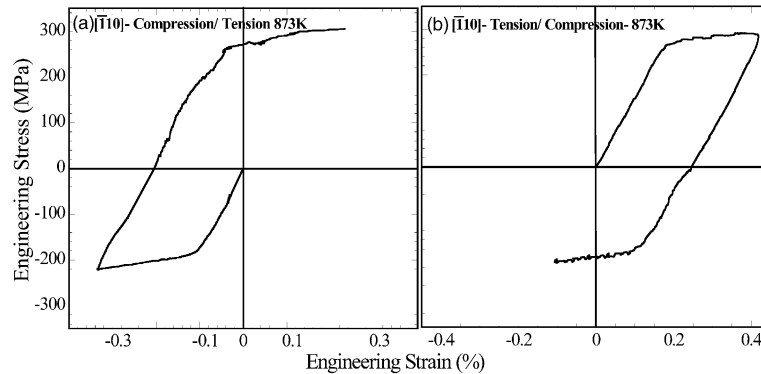


Fig. 11. Cyclic loading curves for the $[\bar{1}\ 1\ 0]$ orientation at 873 K. (a) The first specimen yielded at 219 MPa in compression and then 300 MPa in tension. (b) The second test resulted in the sample yielding in 284 MPa in tension and then 206 MPa in compression.

4.1. Yielding behavior summary

The experimentally measured yielding response of Al-rich single crystalline γ -TiAl can be summarized as follows:

- i) For the three orientations examined in this study γ -TiAl exhibits a positive flow strength dependence on temperature up to a peak, after which the flow strength drops dramatically.
- ii) The $[0\ 0\ 1]$ compressive strength is greater than the tensile strength, and the onset of anomalous yielding occurs at a lower temperature in compression.
- iii) The $[0\ 1\ 0]$ tensile strength is greater than the compressive strength, and the onset of anomal-

ous yielding occurs at a lower temperature in compression.

- iv) The $[\bar{1}\ 1\ 0]$ tensile strength is greater than the compressive strength, but the onset of anomalous yielding occurs at a lower temperature in tension.
- v) In reversed-cycle tests the flow strength depends on the orientation, test temperature, and sense of applied load, but not the sequence of the loading.

4.2. Dislocation core effects

TEM experiments have associated cross-slip locked screw-oriented superdislocations with anomalous yielding in Al-rich single crystalline γ -

TiAl [15,19–25,29]. The prevalence of superdislocation activity and the similarity of the $L1_0$ and $L1_2$ structures suggests that anomalous yielding in γ -TiAl and γ' -Ni₃Al may arise from a common origin. Greenburg et al. [38] proposed a number of non-planar sessile configurations for superdislocations in γ -TiAl. To link the proposed dislocation barriers to yielding, the stability of the core configurations and the mechanisms for the glissile to sessile transformation must be understood.

Atomistic calculations of non-planar “locked” dislocation configurations in γ -TiAl by Woodward et al. [6,39] indicate that acute angle “roof-type” barriers have the largest thermodynamic driving force; with the total energy of the cross-slipped configuration being significantly lower than the planar one. The calculations show that for γ -TiAl a Kear-Wiltsdorf-type lock, similar to that responsible for the yield strength anomaly in Ni₃Al, has an energetic driving force less than half of the “roof-type” barriers [6,39]. The predictions of acute angle dislocation core structures are consistent with experimental high-resolution electron microscopy observations by Hemker et al. [40] and Wang et al. [24].

For cross-slip to occur mixed character Shockley partial dislocations must recombine into a superpartial of pure screw character. Dislocation core spreading determines the height of the cross-slip energy barrier, with the fault energy being inversely proportional to the cross-slip locking activation energy. Applied stress and crystal geometry also have a significant effect on the recombination of partial dislocations and the subsequent cross-slip. Bonneville and Escaig [41] first showed that the resolved shear stress on a dissociated FCC dislocation will either force the two partial dislocations apart, inhibiting cross-slip, or force them together, promoting cross-slip. Paidar et al. [30] have modified Schmid’s law to incorporate “Escaig forces” and successfully predict the orientation dependence and tension/compression asymmetry of the CRSS of Ni₃Al. Moreover, Yoo [42] solved the force balance between the partial dislocations in the framework of anisotropic elasticity and showed that out-of-plane forces produce a torque that pushes the dislocation off the octahedral glide plane. The so-called “Yoo torque” is

pronounced for materials with high elastic anisotropy, and has been shown to be a significant factor in determining the cross-slip frequency of dislocations in Ni₃Al. Here, the influence of crystal geometry, sense of the applied load, the Escaig force and the Yoo torque on the recombination and subsequent cross-slip locking of superdislocations in γ -TiAl is analyzed and used to explain the experimentally measured flow strength anomaly and tension/compression asymmetry.

4.3. Crystallographic considerations

The direction that a dislocation glides is dependent on the orientation and sense of the applied load. The slip systems with the maximum resolved shear stress for each of the three orientations have been analyzed to determine the direction a dislocation travels on the slip plane and the leading stacking fault, i.e. SISF or CSF, as a function of applied load. Superdislocations for each of the three primary slip systems are represented by the Thompson notation [43], and their direction of motion is indicated in Fig. 12.

For the [0 0 1] orientation a tensile shear stress drives the dislocation to the left on the diagram with the CSF on head, Fig. 12(a). Reversing the sense of applied load moves the same dislocation to the right, with the SISF leading. Similarly Fig. 12(b) and (c) present the directions of motion for superdislocations for the near [0 1 0] and $[\bar{1} 1 0]$ orientations. Inspection of this figure shows that in the latter cases a SISF leads during tensile loading and a CSF under compression. If the sign of the dislocation Burgers vector is reversed, both the order of the faults and the direction of motion switch.

The experimental finding that the tension/compression asymmetry is the same for [0 1 0] and $[\bar{1} 1 0]$ but the opposite for [0 0 1] is consistent with the description of dislocation motion outlined in Fig. 12. It is, however, important to note that in all cases the strength is lowest when the CSF leads the dislocation. This finding indicates that the constriction and cross-slip of the leading superpartial dislocation does not have a strong influence on the yield strength anomaly. Since constriction and cross-slip of the leading SISF dissociated superpar-

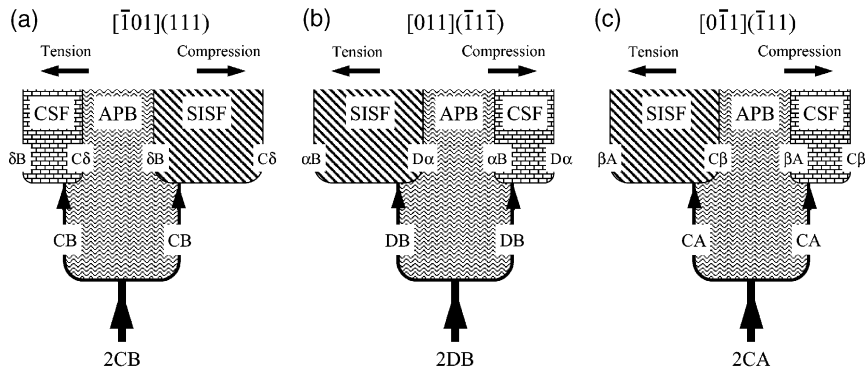


Fig. 12. Schematic drawing of the crystallographic dissociation of superdislocations associated with loading axes (a) $[0\ 0\ 1]$, (b) $[0\ 1\ 0]$ and (c) $[-1\ 1\ 0]$. The drawings and notation given here follow the definition of the Thompson tetrahedron. The direction of motion of these dislocations, with respect to the sense of the applied load (tensile vs. compressive), is presented at the top of the figure and can be used to determine when a CSF leads the dislocation and when it is led by an SISF.

tial is unlikely, the formation of roof-type barriers may in fact be governed by the back cross-slip of the trailing CSF dissociated superpartial.

The CRSS values for the three conditions where the CSF trails, $[0\ 0\ 1]_C$, $[0\ 1\ 0]_T$ and $[-1\ 1\ 0]_T$, are plotted in Fig. 13. The flow strength for each of these conditions was found to be higher than for their tensile or compressive counterparts, and plotting them together illustrates the fact that the data of these “hard” orientations collapse to a single curve. The fact that the CRSS is the same for all three orientations implies that Schmid’s law is obeyed when the asymmetry of superdislocation motion is accounted for. Moreover, the observation

that the anomalous yielding peaks occur at the same temperature for these “hard” orientations points to the activity of a single deformation mechanism, presumably the cross-slip locking of superdislocations by the formation of roof-type barriers.

CRSS values for the conditions where the CSF leads, $[0\ 0\ 1]_T$, $[0\ 1\ 0]_C$ and $[-1\ 1\ 0]_C$, are plotted in Fig. 14. For these “weak” orientations the CRSS do not collapse to a single curve. The magnitude of the flow strength anomaly is approximately the same, but the peak temperature for $[0\ 1\ 0]$ is lower than for $[0\ 0\ 1]$ and $[-1\ 1\ 0]$. This observation

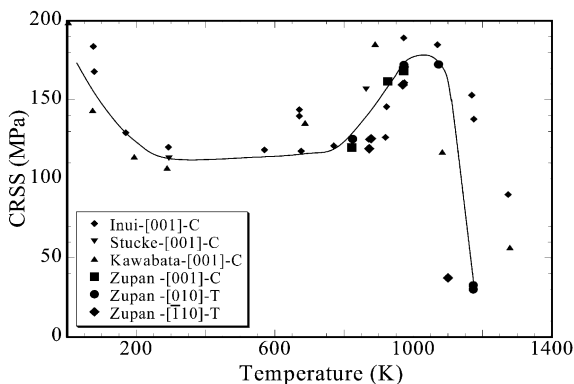


Fig. 13. Plot of the CRSS for the hard directions. The data for these directions converge to a single CRSS and have the same peak temperature for the flow strength anomaly.

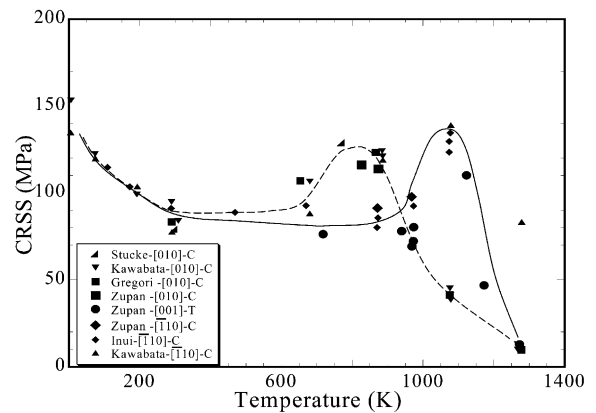


Fig. 14. The CRSS for the three weak orientations. This data does not converge to a single CRSS. The peak temperature of the anomaly for the $[0\ 1\ 0]$ orientation was measured to be much lower than that of the $[0\ 0\ 1]$ and $[-1\ 1\ 0]$ loading axes.

implies that the thermal activation barrier for cross-slip is lower for the near $[0\ 1\ 0]$ loading axis. The fact that the overall strength is lower than for the hard orientations and that the $[0\ 1\ 0]$ behaves differently than the other two orientations suggest that an obstacle other than roof-type barriers may be responsible for the yield strength anomaly for the soft orientations.

4.4. Effect of resolved shear stresses

Fig. 15 gives the planar geometry for the $[\bar{1}\ 0\ 1](1\ 1\ 1)$ slip system that would be active for the $[0\ 0\ 1]$ loading axis. The resolved shear stresses (RSS) for the primary and secondary octahedral slip planes and the cube cross-slip plane are indicated on this figure. Under compressive loading the dislocation glides to the right, and the RSS on the secondary octahedral plane acts to drive back cross-slip of the CSF into an acute angle roof-type barrier, Fig. 15(c), which is in agreement with predictions [6,39] and experimental observations [15,24,40] of superdislocations in γ -TiAl. In tension, the dislocation moves to the left and the RSS on the secondary octahedral promotes the formation of a high-energy non-planar configuration with a CSF located on the cross-slip plane, Fig. 15(b). Similar analysis shows the formation of “roof-

type” barriers is also favored for $[0\ 1\ 0]$ and $[\bar{1}\ 1\ 0]$ tensile loading. The finding that the resolved shear stress promotes cross-slip of the trailing CSF dissociated superpartial dislocations is in agreement with weak-beam TEM observations [15] and the fact that the formation of roof-type barriers occurs when the sense of the applied load is in the hard direction.

4.5. Effect of the Yoo torque

Yoo and Fu [14] have calculated the anisotropic interaction forces on dissociated screw dislocations in γ -TiAl. For the $[\bar{1}\ 0\ 1](1\ 1\ 1)$ slip system illustrated in Fig. 15, the tangential force from crystal anisotropy push the CSF dissociated superpartial off the slip plane in the $[1\ 1\ 1]$ direction. Calculations made using the codes of Yoo and Fu [14] show the stress on the superpartial to be approximately 300–600 MPa depending on the SISF and APB energies. The magnitude of the stresses associated with the Yoo torque is substantially larger, more than three times, than the RSS on the cross-slip planes. By comparison, the Yoo torque results in a stress of 540 MPa in Ni_3Al [31], but the yield strength of Ni_3Al is much higher and the RSS are comparable to the torque stress for Ni_3Al . For γ -TiAl, the large magnitude of the Yoo torque com-

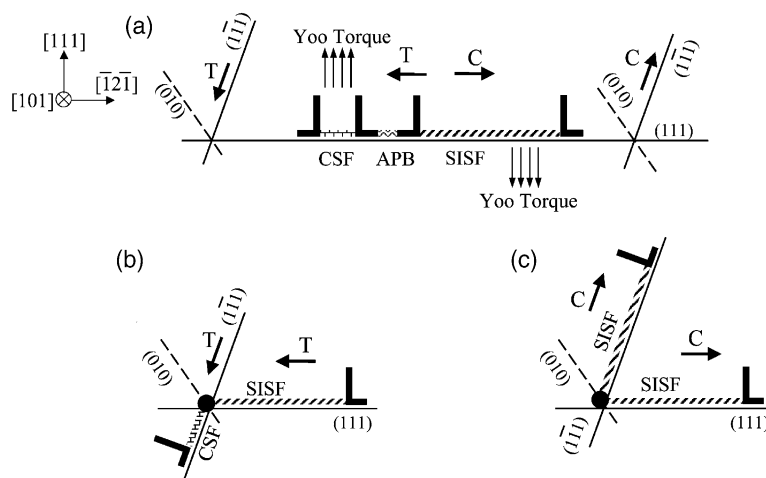


Fig. 15. Schematic of a $[\bar{1}\ 0\ 1]$ superdislocation gliding on the $(1\ 1\ 1)$ plane displaying the motion of the dislocation when the crystal is loaded in tension or compression for orientations near $[0\ 0\ 1]$. Under a compressive load, the trailing CSF dissociated superpartial dislocations can cross-slip on to a second octahedral plane forming an acute angle “roof-type” barrier.

pared to the RSS significantly increases its effect on the cross-slip locking of superdislocations.

The Yoo torque, like the RSS, promotes the formation of the low energy “roof-type” barrier through cross-slip of the trailing CSF dissociated superpartial dislocation in each of the hard orientations ($[0\ 0\ 1]_C$, $[0\ 1\ 0]_T$ and $[\bar{1}\ 1\ 0]_T$). This finding further supports the supposition that the formation of roof-type barriers leads to anomalous yielding in γ -TiAl. The elastic anisotropy interaction force does not change with the orientation or applied load and can be used to explain the adherence to Schmid’s law illustrated in Fig. 13. The Yoo torque in effect, mitigates the importance of the secondary RSS. The Yoo torque acts against the RSS in the soft orientations ($[0\ 0\ 1]_T$, $[0\ 1\ 0]_C$ and $[\bar{1}\ 1\ 0]_C$) and appears to lead to the formation of an alternative, unidentified but less formidable, barrier.

4.6. Escaig forces on partial dislocation constriction

Following the work of Bonneville and Escaig [41], Paidar et al. [30] considered the geometry of a fourfold dissociated superpartial dislocation in Ni_3Al and formulated the following equation for the Escaig effect on the CSF separation of a pair of Shockley partial dislocations on the primary slip plane

$$d_p = \frac{d_o}{\left[1 - \left(\frac{\gamma_{APB}}{2\gamma_{CSF}} + \frac{\tau_{pe}b}{2\sqrt{3}\gamma_{CSF}} \right) \right]} \quad (2)$$

The unstressed dislocation spacing is d_o , b is the Burgers vector, γ_{APB} and γ_{CSF} are the APB and CSF fault energies and τ_{pe} the resolved shear stress on the edge component of the Shockley partial dislocation. This relation was adapted for γ -TiAl using the asymmetrical geometry and appropriate values for the APB and fault energies in γ -TiAl, and the results of this analysis indicate that, unlike Ni_3Al , the applied stress has little or no effect on the magnitude of the CSF dissociation in γ -TiAl. This finding seems reasonable in light of its high CSF energy and is consistent with atomistic calculations of Woodward and MacLaren [39], which predict

that neither the Escaig stress nor the RSS have a strong effect on the driving force for cross-slip in γ -TiAl. The conclusion that the Escaig force does not play a major role in the cross-slip locking of superdislocation in γ -TiAl is also in good agreement with the measured adherence to Schmid’s law shown in Fig. 13.

5. Concluding remarks

The flow response of Al-rich single crystalline γ -TiAl has been investigated as a function of crystallographic orientation, sense of the applied load and temperature. Anomalous yielding and a tension/compression asymmetry were measured for each of the crystallographic orientations studied, namely the $[0\ 0\ 1]$, $[0\ 1\ 0]$ and $[\bar{1}\ 1\ 0]$. The location of the anomalous peak and the direction of the tension/compression asymmetry were found to be orientation dependent. The tensile yield strength was measured to be stronger compared compressive yielding for the $[0\ 1\ 0]$ and $[\bar{1}\ 1\ 0]$ orientations whilst the opposite was found for the $[0\ 0\ 1]$ direction.

A micromechanical model based on superdislocation cross-slip has been developed to explain the observed tension/compression asymmetries. Separating the flow strength data with regard to the direction of dislocation motion has illustrated that the CRSS is lowest when the CSF leads and highest when it trails. Schmid’s law violations were not observed for the case when the CSF trails. The Yoo torque and RSS on the cross-slip plane were both found to promote the formation of low energy acute angle “roof-type” barriers through back cross-slip of the trailing CSF dissociated superpartial dislocation. Escaig constriction forces have been evaluated and found to have little or no effect on the CSF dissociation. Mitigation of the Escaig forces and the fact that the Yoo torque is much higher than the secondary RSS combine to explain why γ -TiAl does not show significant violations of Schmid’s law. The lower strengths and variations in the onset of anomalous yielding associated with the case where the CSF leads the superdislocation is believed to be related to the creation of a less formidable, but as of yet unidentified, locked configuration.

Acknowledgements

The National Science Foundation provided financial support for this study. The authors are especially grateful for illuminating discussions and computational assistance that was graciously provided by Dr. Man Yoo.

References

- [1] Huang SC, Chesnutt JC. In: Westbrook JH, Fleischer RL, editors. Intermetallic compounds. New York, USA: John Wiley & Sons Ltd; 1994, p. 73–90.
- [2] Kim Y-W. In: Kim YW, Wagner R, Yamaguchi M, editors. Gamma titanium aluminides. The Minerals, Metals and Materials Society; 1995, p. 637–54.
- [3] Mehl MJ, Osburn JE, Papaconstantopoulos DA, Klein BM. In: Stocks GM, Pope DP, Giamei AF, editors. Alloy phase stability and design symposium, 186. Materials Research Society; 1991, p. 277–82.
- [4] Tanaka K, Ichitsubo T, Inui H, Yamaguchi M, Koiwa M. *Philos Mag Lett* 1996;73:71–8.
- [5] Fu CL, Yoo MH. *Philos Mag Lett* 1990;62:159–65.
- [6] Woodward C, MacLaren JM, Dimiduk DM. In: Baker I, Darolia R, Whittenberger JD, Yoo MH, editors. High-temperature ordered intermetallic alloys V, 288. Materials Research Society; 1993, p. 171–6.
- [7] Simmons JP, Rao SI, Dimiduk DM. In: Baker I, Darolia R, Whittenberger JD, Yoo MH, editors. High-temperature ordered intermetallic alloys V, 288. Materials Research Society; 1993, p. 335–42.
- [8] Rao S, Woodward C, Dimiduk DM. In: Horton JA, Baker I, Hanada S, Noebe RD, Schwartz DS, editors. High-temperature ordered intermetallic alloys VI, 364. Materials Research Society; 1995, p. 129–36.
- [9] Panova J, Farkas D. In: Kim YW, Wagner R, Yamaguchi M, editors. Gamma titanium aluminides. Warrendale, PA: TMS; 1995, p. 331–8.
- [10] Girshik A, Vitek V. In: Horton JA, Baker I, Hanada S, Noebe RD, Schwartz DS, editors. High temperature ordered intermetallic alloys VI, 364. Materials Research Society; 1995, p. 145–50.
- [11] Schoeck G, Ehmann J, Fahnle M. *Philos Mag Lett* 1998;78:289–95.
- [12] Hug G, Loiseau A, Veyssiere P. *Philos Mag A* 1988;57:499–523.
- [13] Wiezorek JMK, Humphreys CJ. *Scripta Metall Mater* 1995;33:451–8.
- [14] Yoo MH, Fu CL. *Metall Mater Trans A* 1998;29:49–63.
- [15] Gregori F, Veyssiere P. *Mater Sci Eng A* 2001;309:310:87–91.
- [16] Kawabata T, Kanai T, Izumi O. *Acta Metall* 1985;33:1355–66.
- [17] Kawabata T, Abumiya T, Kanai T, Izumi O. *Acta Metall Mater* 1990;38:1181–393.
- [18] Kawabata T, Kanai T, Izumi O. *Philos Mag A* 1991;63:1291–8.
- [19] Kawabata T, Kanai T, Izumi O. *Philos Mag A* 1994;70:43–51.
- [20] Inui H, Matsumuro M, Wu D-H, Yamaguchi M. *Philos Mag A* 1997;75:395–423.
- [21] Stucke MA, Dimiduk DM, Hazzledine PM. In: Baker I, Darolia R, Whittenberger JD, Yoo MH, editors. High-temperature ordered intermetallic alloys V, 288. Materials Research Society; 1993, p. 471–6.
- [22] Stucke MA, Vasudevan VK, Dimiduk DM. *Mater Sci Eng* 1995;A192/193:111–9.
- [23] Wang Z-M, Li ZX, Whang SH. *Mater Sci Eng* 1995;A192/193:211–6.
- [24] Wang Z-M, Wei C, Feng Q, Whang SH, Allard LF. *Intermetallics* 1998;6:131–9.
- [25] Jiao S, Bird N, Hirsch PB, Taylor G. *Philos Mag A* 1998;78:777–802.
- [26] Viguier B, Hemker KJ, Bonneville J, Louchet F, Martin J. *Philos Mag A* 1995;71:1295–312.
- [27] Sriram S, Vasudevan VK, Dimiduk DM. *Mater Sci Eng* 1995;A192/193:217–25.
- [28] Bird N, Taylor G, Sun YQ. In: Horton JA, Baker I, Hanada S, Noebe RD, Schwartz DS, editors. High temperature ordered intermetallic alloys VI, 364. Materials Research Society; 1995, p. 635–40.
- [29] Feng Q, Whang SH. *Intermetallics* 1999;7:971–9.
- [30] Paidar V, Pope DP, Vitek V. *Acta Metall* 1984;32:435–48.
- [31] Umakoshi Y, Pope DP, Vitek V. *Acta Metall* 1984;32:449–56.
- [32] Sharpe Jr. WN. *Optical Eng* 1982;21:483–8.
- [33] Sharpe Jr WN. An interferometric strain/displacement measurement system. Mechanics and Materials Branch NASA Langley Research Center, Report 101638; 1989.
- [34] Zupan M, Hayden MJ, Boehlert CJ, Hemker KJ. *Exp Mech* 2001;41(3):242–7.
- [35] Zupan M, Hemker KJ. *Exp Mech* 2002;42(2):214–21.
- [36] He Y, Schwarz RB, Darling T, Hundely M, Whang SH, Wang SC. *Mater Sci Eng* 1997;A239–240:157–63.
- [37] Zupan M, Hemker KJ. High temperature microsample tensile testing of γ -TiAl. *Mater Sci Eng A* 2001;319:321:810–4.
- [38] Greenberg BA, Antonova OV, Indenbaum VN, Karkina LE, Notkin AB, Ponomarev MV. *Acta Metall Mater* 1991;39:233–42.
- [39] Woodward C, MacLaren JM. *Philos Mag A* 1996;74:237–357.
- [40] Hemker KJ, Viguier B, Mills MJ. *Mater Sci Eng A* 1993;164:391–4.
- [41] Bonneville J, Escaig B. *Acta Metall* 1979;27:1477.
- [42] Yoo MH. *Acta Metall* 1987;35:1559–69.
- [43] Hirth JP, Lothe J. In: Theory of dislocations. New York: McGraw-Hill Book Company; 1968, p. 780.